Article

Passivating Nucleobases Bring Charge Transfer Character to Optically Active Transitions in Small Silver Nanoclusters

Mohammed A. Jabed, Naveen Dandu, Sergei Tretiak, and Svetlana Kilina*

Read Online

ACCESS | 📊 Metrics & More | 📄 Article Recommendations | 📑 Supporting Information

ABSTRACT: DNA-wrapped silver nanoclusters (DNA−AgNCs) are known for their efficient luminescence. However, their emission is highly sensitive to the DNA sequence, the cluster size, and its charge state. To get better insights into photophysics of these hybrid systems, simulations based on density functional theory (DFT) are performed. Our calculations elucidate the effect of the structural conformations, charges, solvent polarity, and passivating bases on optical spectra of DNA−AgNCs containing five and six Ag atoms. It is found that inclusion of water in calculations as a polar solvent media results in stabilization of nonplanar conformations of base-passivated clusters, while their planar conformations are more stable in vacuum, similar to the bare Ag_5 and Ag_6 clusters. Cytosines and guanines interact with the cluster twice stronger than thymines, due to their larger dipole moments. In addition to the base−cluster interactions, hydrogen bonds between bases notably contribute to the structure stabilization. While the relative intensity, line width, and the energy of absorption peaks are slightly changing depending on the cluster charge, conformations, and base types, the overall spectral shape with five well-resolved bands at 2.5−5.5 eV is consistent for all structures. Independent of the passivating bases and the cluster size and charge, the low energy optical transitions at 2.5−3.5 eV exhibit a metal to ligand charge transfer (MLCT) character with the main contribution emerging from Ag-core to the bases. Cytosines facilitate the MLCT character to a larger degree comparing to the other bases. However, the doublet transitions in clusters with the open shell electronic structure (Ag_5 and Ag_6^+) result in appearance of additional red-shifted (<2.5 eV) and optically weak band with negligible MLCT character. The passivated clusters with the closed shell electronic structure (Ag_5^+ and Ag_6) exhibit higher optical intensity of their lowest transitions with much higher MLCT contribution, thus having better potential for emission, than their open shell counterparts.
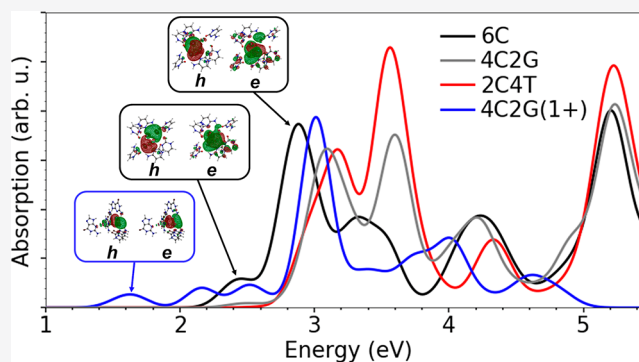
INTRODUCTION

Silver clusters of a few atoms (<25) in size behave as fluorescent emitters when coordinated and stabilized by a single-stranded DNA.[1] Oligonucleotides typically with 10−30 bases locally concentrate Ag^+ cations[2] and facilitate assembly of chemically reduced silver in a form of nanoclusters encapsulated in DNA (DNA−AgNCs).[3−9] Such DNA−AgNCs demonstrate emission at the range from visible to near-infrared wavelength with high quantum yields[2,10] up to 90% and lifetimes of 1−5 ns.[1,11−14] These data demonstrate that DNA−AgNCs have excellent optical properties, accompanied by high photostability and low toxicity, which make them even more appealing in biological applications compared to organic dyes and semiconductor quantum dots.[15−19] Technological applications of DNA−AgNCs include their use as highly sensitive sensors,[20−22] fluorophores in bioimaging[23,24] (especially beneficial at high background interferences[25]), and in vitro and in vivo nanothermometry.[26]

However, the structural and optical properties of DNA−AgNCs have proven to be challenging to control, as they can adopt a wide variety of shapes, sizes, charges, and conformations, which change with the DNA sequence[1] and its secondary structure.[12,27−31] The molecule-like (discrete) electronic structure of DNA−AgNCs is very sensitive to variations in their conformations, oxidation state, and binding sites interacting with DNA bases leading to significantly different optical and catalytic properties of specific clusters.[32,33] In particular, DNA−AgNCs usually exhibit multiple absorption and emission peaks that do not correlate well to structured continuum features.[27,34] The variations in emission wavelength upon changes in the excitation wavelength together with the increase of the average decay time as a function of wavelength in DNA−AgNCs[35] have been related to different emitters due to inhomogeneous changes of the conformation of the AgNC
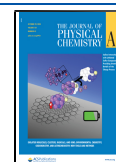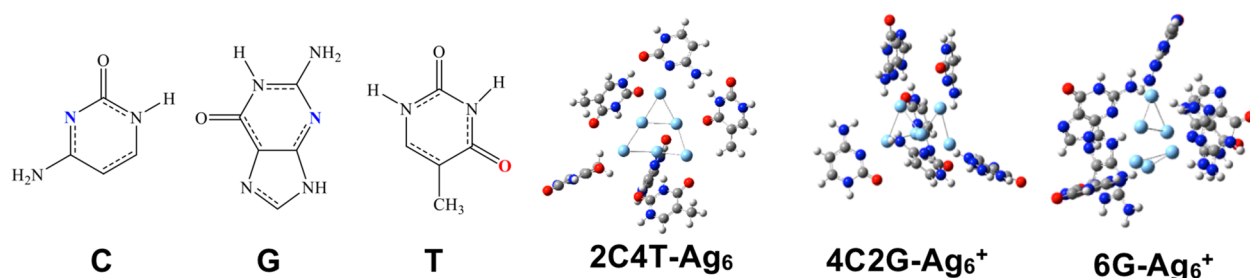
Figure 1. Chemical structures of three DNA bases, cytosine (C), guanine (G), and thymine (T), and examples of optimized geometries of charged and neutral Ag$_6$ clusters passivated by a different number of C, G, and T bases. The colored atoms in the schematic representation of bases indicate the atoms coordinated to silver atoms in DNA−AgNCs.

or the DNA scaffold.[36,37] Nonetheless, it was also found that certain shapes and sizes of AgNCs are more stable at a given DNA length,[38−40] sequence,[1,2,4,10,13,27,29,41,42] and synthesis conditions, including variations in Ag$^+$ concentrations,[3,43] pH,[43,44] and types of oxidizing−reducing agents.[1,45]

As such, the stoichiometry of AgNC and, consequently, their electronic structure and optical spectra can be controlled to some degree by altering the DNA sequences. For instance, it is reported that Watson−Crick type pairing through Ag$^+$ bridging can stabilize the double-stranded DNA and form elongated nanorod clusters.[27,46,47] Single-stranded DNA typically results in brighter DNA−AgNCs by forming loops around the cluster.[1,48] It was recently detected that different lengths of repeated DNA strands form a minimal $(C_2X)_6$ (where C = cytosine and X = guanine, adenine, or thymine) scaffold that stabilizes the $(Ag_{10})^{6+}$ chromophore absorbing between 400−450 nm.[49] This suggests that AgNCs of a certain stable stoichiometry can be coordinated via multiple nucleobases.

In the case of homo-oligonucleotide, cytosine (C)[13,43,50] and guanine (G)[50] strands have been reported to form highly emissive DNA−AgNCs. Clusters composed of thymine (T) strands emit only at the controlled oxidation state,[45,50] while adenine (A) strands do not result in emissive clusters.[39,50] Therefore, adenine (A) is typically used as a spacer between nucleotide sequences. Calculations also support these results predicting higher affinity of the cationic silver to C[51] and G[52] nucleotides forming coordinated bonds with their nitrogens.[53] Similar to the emission energies, the intensity of the emission also depends on cluster−base interactions. Due to the highest reduction potential among nucleotide bases, G−Ag interaction could increase the hybridized charge transfer character of the lowest energy transitions, which is expected to improve the intensity of the emission.[39,54] Despite these extensive studies, identification and controllable manipulation of the structure, size, and shape of DNA−AgNCs are still disputed. Overall, the rigorous relationships between structural conformations and optical response of DNA−AgNCs are yet to be established.

Complementing experiments, quantum chemistry calculations based on density functional theory (DFT) are able to provide important insights into the interaction mechanisms between the DNA bases and AgNCs and their effect on the geometry, electronic structure, and optical response of a hybrid system. It is well understood that the symmetry of the metal clusters[56] is modified significantly by polar solvents and DNA−metal interactions. However, literature reports on such simulations are still incomplete. Reported studies are mainly focused on the impact of a charge and/or a size of small AgNCs (of two to six atoms in size) on the interaction with a specific DNA base (either C[51] or G[52,55]). The effect of a base

type on the interaction with AgNCs has been also studied computaionally.[51,52] In all cases, however, the stability and optical spectra of DNA−AgNC have been modeled for clusters bound to only one type or a pair of bases in vacuum, rather than clusters completely encapsulated by different bases in a polar media, as it takes place in experiments. Samanta et al.[57] have reported the importance of inclusion of a complete nucleotide model, where a single-stranded DNA consisted of only identical nucleobases encapsulating Ag$_{12}$ clusters. However, in this study optical spectra are obtained based on the ground-state density matrix. An accuracy of this simplistic approach is in question when the electronic correlation effects, such as the exciton binding energy, are large as in small metal clusters.[58]

Motivated by the idea of improving the DNA−AgNCs models to better suit realistic structures, here we present DFT and time-dependent DFT (TDDFT) calculations of AgNCs fully passivated by various DNA bases, including their mixtures, in a polar environment and compare results to the vacuum calculations. We focus on small AgNCs models of five and six atoms in size, which have already been simulated.[59] Complementing previous studies, we include complete encapsulation of clusters with different combinations of C, G, and T passivating agents, as illustrated in Figure. 1. We also elucidate the effect of conformations, charges, and a polar solvent on the optical spectra of DNA−AgNCs. We have focused only on neutral and +1 charged Ag$_5$ and Ag$_6$ clusters, because they reproduce two cases for spin multiplicity: singlets for Ag$_6$ and Ag$_5^+$ versus doublets for Ag$_5$ and Ag$_6^+$. Thus, these cases allow comparison between nearly the same size clusters with different charges and spin multiplicity. Our calculations have shown that the spin multiplicity affects the lowest energy transitions more strongly, compared to effects of the charge or cluster size. Inclusion of a polar media, such as water, drastically changes both the cluster shape and optical spectra of DNA−AgNCs. The lowest optical transitions mainly have a charge transfer (CT) character with a dominant contribution from the Ag-core to the bases, with C facilitating the CT character to a larger degree compared to G and T bases, including the mixed nucleobase passivation. While the relative intensity, line width, and energy of the optical peaks slightly change depending on the cluster charge, conformations, and base types, the overall spectral shape with five well-resolved bands is consistent for all structures.

■ METHODOLOGY AND COMPUTATIONAL DETAILS

Models of AgNC Structures. Initial geometries of our DNA−AgNCs are created using several low energy conformations of bare Ag$_5$ and Ag$_6$ clusters reported in the

literature.[60] The lowest energy conformations of bare AgNCs smaller than seven atoms in size have been proven to have planar geometries.[56,59,60] To check the effect of planarity of DNA−AgNCs, we also model nonplanar low energy conformations of Ag_6 and Ag_5 as initial structures (Table 1).

Table 1. Most Stable Ag_6 and Ag_5 Clusters Used as Initial Structures for Related Isomers of 6C−Ag_6 and 5C−Ag_5 DNA−AgNCs Optimized in Vacuum and Water with No Charge (neutral) and +1 Charge[a]

	Initial AgNC structure	Optimized Neutral		Optimized Charged	
		Vacuum	Water	Vacuum	Water
Ag_6 clusters	Geom-1 / 0.00 eV	0.00 eV	0.00 eV	0.00 eV	0.00 eV
	Geom-2 / 0.20 eV	0.88 eV	0.13 eV	0.01 eV	0.26 eV
	Geom-3 / 0.84 eV	1.29 eV	-0.12 eV	-0.18 eV	-0.11 eV
Ag_5 clusters	Geom-1 / 0.00 eV	0.00 eV	0.00 eV	0.00 eV	0.00 eV
	Geom-2 / 0.99 eV	-0.31 eV	-0.13 eV	0.41 eV	0.01 eV
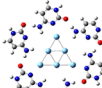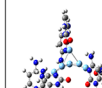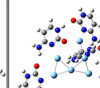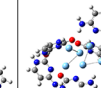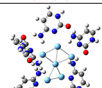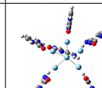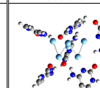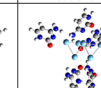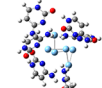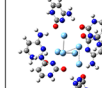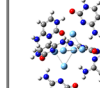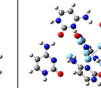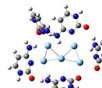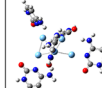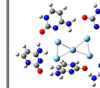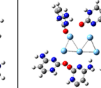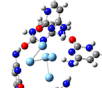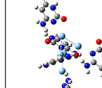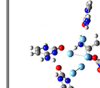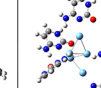
[a]Zero energy is assigned to structures with the lowest energy of their bare AgNC counterparts. The red font depicts the optimized final structures with the lowest energies among considered isomers.

Because all Ag atoms in such clusters can be considered as surface atoms, the DNA bases are then added to each Ag atom of the cluster and optimized with (+1 e) and without charge (neutral). Using this approach, we have constructed clusters passivated by only C, G, or T (5X−Ag_5 and 6X−Ag_6, with X = C, G, or T) and by their combinations of (n−2)C2X−Ag_n and 2C(n−2)T−Ag_n, where n = 5 or 6 and X = G or T.

Calculations of Optimized Geometries and Optical Spectra. DFT is applied for geometry optimization of all considered DNA−AgNCs. TDDFT[61,62] is used for all excited-state calculations, as implemented in Gaussian-09 software package.[63] Long-range corrected exchange-correlation functional CAM-B3LYP[64] and mixed basis set LANL2DZ[65] (for Ag atoms) and 6-31G*[66] (for N, O, C, and H atoms) are used for both the ground- and excited-state calculations. The long range corrected CAM-B3LYP functional has shown more accurate description of charge transfer transitions in DNA−AgNCs, compared to pure GGA or hybrid functionals, despite consistent blue-shifts in optical transitions.[67−69] These findings define our choice of the functionals and basis sets. In addition to vacuum calculations, we have also performed calculations in water utilizing a conductor-like polarizable continuum model (CPCM)[70] for simulating a solvent environment for the ground- and excited-state calculations. Starting with three

different initial geometries (Table 1) for optimization helps to chose the confirmation with the lowest energy that is then used for calculations of optical spectra.

Ninety optical transitions are obtained from TDDFT calculations to reproduce the absorption spectra in the range of 1.00−5.50 eV. The profile of the spectra is modeled using the Gaussian function with the width of 0.08 eV to reproduce a thermal broadening of spectral bands. To visualize the charge density distribution of calculated excited states, natural transition orbitals (NTOs)[71] are analyzed for photoexcited electron−hole pair based on transition densities obtained from TDDFT, as implemented in Gaussian-09[63] software. VMD[72] software has been used for visualization of NTOs. To better understand the nature of the transitions, we have decomposed the excited-state wave function contributed from the Ag and the base parts of the DNA−AgNCs and plotted it as a difference between the electron and hole states, as explained in Supporting Information (eqs i−vii).

Calculations of AgNC−Base Binding Energies. To estimate the strength of interaction between the specific type of the base (L_1 = C, G, or T) and the AgNC, the binding energy is calculated using the following formulas:

$$E_{b,L1} = \frac{(E_{Ag_n L1_p L2_q} - E_{Ag_n L2_q} - p*E_{L1})}{p} \quad (1)$$

where n is the number of the silver atoms, p and q are the number of the base types L_1 and L_2, respectively, with $n = p + q$. The energy $E_{Ag_n L2_p}$ is calculated for an optimized DNA−AgNCs fragment with the bases of type L_1 removed from the AgNC. The energy E_{L1} is calculated for the isolated optimized base of the type L_1. For clusters passivated only by cytosines, the average cluster−base binding energy, ⟨Ag−N⟩, is calculated as the difference between the total energies of the passivated cluster and its pristine counterparts (i.e., the bare silver cluster and the pristine cytosine multiplied by the number of cytosines at the cluster), with all structures optimized to their minimal energies. To obtain the average binding energy per base, the final result is divided by the total number of cytosines passivating the cluster. The negative value of binding energy means stabilization favoring hybrid species formation due to binding.

■ RESULTS AND DISCUSSION

Structural Features of Clusters Passivated by Cytosines. Due to a high degree of flexibility of the nucleotides passivating DNA−AgNCs, different structural conformations of clusters likely coexist in experimental samples. To address the diversity in DNA−AgNC conformations, we consider both planar and nonplanar geometries of Ag_5 and Ag_6 clusters that have been shown as one of the most stable conformers of bare silver clusters of these sizes.[60,73] DNA−AgNCs of 5C−Ag_5 and 6C−Ag_6 initially constructed from these bare clusters are used to study the effect of a polar solvent, charge, and passivating bases on the structural conformations of clusters, with results presented in Table 1. In vacuum, coordination of Ag atoms by cytosines noticeably changes the geometry of nonplanar neutral clusters (Geom-2 and Geom-3), while only slightly distorting the initially planar conformation (Geom-1). The cluster 6C−Ag_6 stays planar to preserve its $^1D_{3h}$ symmetry, resulting in the lowest energy conformation among its isomers. However, a slight distortion results in breaking a perfect planarity of the cluster 5C−Ag_5

Table 2. Structural Parameters of the 6C–Ag$_6$ Cluster[a]

6C–Ag$_6$ isomers			vacuum			solvent		
			Geom-1	Geom-2	Geom-3	Geom-1	Geom-2	Geom-3
neutral	bond length (Å)	$\langle$Ag–Ag$\rangle$	2.78 ± 0.02	2.77 ± 0.03	2.86 ± 0.17	2.81 ± 0.05	2.82 ± 0.12	2.85 ± 0.12
		$\langle$Ag–N$\rangle$	3.45 ± 1.17	2.97 ± 0.81	2.71 ± 0.60	2.45 ± 0.07	2.61 ± 0.55	2.44 ± 0.03
		(Ag–N)$_{long}$	4.52	4.03	3.92	2.57	3.75	2.48
		(Ag–N)$_{short}$	2.38	2.33	2.42	2.39	2.36	2.39
	no. of bonds	Ag–N	3	4	5	6	5	6
		H-bond	6	2	4	1	1	4
	E_b, eV	$\langle E_{Ag-N}\rangle$	−0.81	−0.77	−0.80	−0.31	−0.98	−0.55
		$E_{Ag-N,short}$	−1.21	−1.28	−0.45	−0.19	−0.81	−0.29
		$E_{Ag-N,long}$	−1.21	−0.75	−0.33	−0.16	−1.074	−0.28
charged (+1)	bond length (Å)	$\langle$Ag–Ag$\rangle$	2.77 ± 0.06	2.86 ± 0.10	2.84 ± 0.09	2.85 ± 0.09	2.83 ± 0.11	2.87 ± 0.10
		$\langle$Ag–N$\rangle$	2.63 ± 0.55	2.40 ± 0.08	2.36 ± 0.02	2.39 ± 0. 09	2.35 ± 0.03	2.37 ± 0.04
		(Ag–N)$_{long}$	3.74	2.56	2.39	2.55	2.40	2.43
		(Ag–N)$_{short}$	2.30	2.32	2.34	2.30	2.33	2.32
	no. of bonds	Ag–N	5	6	6	6	6	6
		H-bond	4	4	5	3	2	4
	E_b, eV	$\langle E_{Ag-N}\rangle$	−1.19	−1.21	−1.22	−0.57	−1.11	−0.61
		$E_{Ag-N,short}$	−0.52	−0.92	−0.97	−0.35	−0.63	−0.56
		$E_{Ag-N,long}$	−1.20	−0.85	−0.56	−0.21	−0.76	−0.34

[a]For the average silver−silver bond length, $\langle$Ag−Ag$\rangle$, only Ag−Ag bond lengths less than 3 Å are taken into account. For the average Ag−N bond length between the cluster and the base, $\langle$Ag−N$\rangle$, all six bonds are taken into account. The bond between the oxygen and hydrogen of two adjacent cytosines shorter than 2 Å is considered as the hydrogen bond (H-bond). The cluster−base binding energies (E_b) are calculated using eq 1 in the main text, where L_1 is the cytosine with either the shortest or the longest Ag−N bond length and $p = 1$.

raising its energy by ~0.3 eV, compared to its nonplanar isomer (Geom-2). In vacuum, charging the clusters (i.e., switching to cationic species with +1 charge) results in a significant stabilization of the nearly planar Geom-1 isomer of **5C–Ag$_5$$^+$**, while it breaks initial planarity and the symmetry of Geom-1 **6C–Ag$_6$$^+$**, destabilizing this structure, compared to other charged isomers considered.

Several competing factors influence the overall stability of the cluster. It was shown that closed shell small metal clusters are more stable in their symmetric planar structure.[56,74] This agrees with our findings that the planar geometries of the **6C-Ag$_6$** and **5C-Ag$_5$$^+$** are more stable compared to their nonplanar 3-D isomers, Table 1. However, for all structures in vacuum, cytosines are not equally coordinated with Ag atoms, as evidenced from the significant variations in the Ag−N bond lengths mainly correlated to the strength of the binding energy between the base and the cluster, as presented in Table 2 for **6C–Ag$_6$** and Table S1 in SI for **5C-Ag$_5$** clusters. This behavior is the most pronounced for **6C–Ag$_6$** isomers in vacuum. For instance, only three bases create strong coordinate bonds with Ag at the edges of the planar Geom-1 structure, while the other three bases are much more weakly coordinated with Ag at the sides (see Tables 1 and 2). However, weakly coordinated bases form a hydrogen bond (H-bond) with the oxygen from the nearest base, thus encapsulating the cluster and minimizing the total energy of the Geom-1 isomer of **6C–Ag$_6$**. Nonplanar geometry of the clusters breaks some of hydrogen bonds, raising the total energy of 3-D **6C–Ag$_6$** isomers in vacuum. In contrast, the energy of 3-D **6C–Ag$_6$$^+$** is reduced for Geom-3 due to a larger number of hydrogen bonds and also decreased Ag−N bond length for all capping bases associated with the strongest base−cluster interactions. Similar trends are observed for Ag$_5$ in vacuum, where both the nonplanar structure (Geom-2) of **5C–Ag$_5$** and the nearly planar structure (Geom-1) of **5C–Ag$_5$$^+$** feature the maximum number of hydrogen bonds and the

strongest base−cluster interactions resulting in the most stable conformations, Table S1 in SI.

It is important to note that the shortest Ag−N bond does not always correspond to the strongest binding energy between the base and the cluster, Table 2. This discrepancy originates from a strong structural reconstruction of the cluster after removal of the base, when used in calculations of the binding energy according to eq 1. For instance, losing one of bases from the planar isomer (Geom-1) of **6C–Ag$_6$** results in a new **5C–Ag$_6$** structure, where the weakly interacting base is strongly coordinated to the side Ag atom via the nitrogen and also to the edge Ag atom via the oxygen, Figure S1 in SI. As such, the obtained base−cluster binding energy is "contaminated" by the additional interaction via the oxygen that is not presented in the initial structure (also see an extended discussion on this effect in SI). Due to strong structural variations upon removal of one of cytosines, trends in the base−cluster binding energies are not well correlated with the trends in the Ag−N bond lengths for some isomers. On the other hand, the obtained **5C–Ag$_6$** structure demonstrates that cytosines can be coordinated to AgNC via either nitrogen or oxygen or both, if there is a limiting number of bases available for the cluster capping. This result agrees with computational findings for Ag$_{12}$ clusters encapsulated in a single-stranded DNA scaffold consisting of 12 nucleobases.[57]

A polar solvent, such as water, significantly reduces the number of hydrogen bonds in the DNA−AgNCs due to the dipole−dipole screening effect. As a result, all optimized structures in water are not planar and their initial structural symmetry is also significantly distorted, Table 1. Similar to the vacuum calculations, the most stable isomer is the one preserving the largest number of hydrogen bonds and the strongest base−cluster interactions associated with nearly similar Ag−N bond length for all bases. In water, these conditions are satisfied for the Geom-3 isomer of **6C–Ag$_6$** and

$6C-Ag_6^+$ (Tables 1 and 2) and Geom-1 isomer of $5C-Ag_5$ and $5C-Ag_5^+$ (Table S1 in SI).

Calculated structures point to three main trends. First, our results are commensurate with the previous studies of larger clusters (>10 atoms) confirming nonplanar 3-D structures of DNA—AgNCs in polar solvents.[53,75,76] Moreover, our results reveal that a polar solvent governs the planar to nonplanar 3-D structural transition for energy stabilization even for DNA—AgNC isomers with less than seven atoms in size. Second, inclusion of a polar solvent significantly changes the conformation of the DNA—AgNCs by reducing the number of hydrogen bonds between the neighboring bases and making all bases nearly equally interacting with Ag atoms. Both conditions play a key role in stabilization of a particular isomer. Third, several isomers of DNA—AgNCs likely coexist in polar solvents due to the relatively small energy differences between their conformations (0.1–0.2 eV). In contrast, closed shell $6C-Ag_6$ and $5C-Ag_5^+$ clusters in vacuum (or nonpolar solvents) have distinct preferential planar conformations, with larger differences in their total energies (up to ~1 eV) compared to nonplanar isomers, which agrees with computational predictions obtained for the bare Ag clusters.[56,74,77]

Dependence of Optical Properties on Conformations of Clusters Passivated by Cytosines. Absorption spectra of all considered isomers calculated in vacuum and water are shown in Figure 2 for $6C-Ag_6$ and in Figure S2 in SI for 5C—

stable structure, while the Geom-1 isomer features the bright first transition both in vacuum and water, Figure 2c,d. These results suggest that emissive $6C-Ag_6$ clusters in polar solvents are likely charge-neutral. In contrast, both isomers of the charged $5C-Ag_5^+$ cluster demonstrate the narrow and highly intensive lowest peak with optically active first transitions in water, compared to the broader and much less intensive first peak of neutral $5C-Ag_5$ clusters, Figure S2b and S2d in SI. This suggests that charged $5C-Ag_5^+$ clusters (with the closed shell electronic structure) are expected to be more emissive in polar solvents compared to their neutral counterparts (open shell structures).

The overall line-shape of absorption spectra of clusters, however, is not very sensitive to the geometry of isomers, with less pronounced changes in spectral features for both charged and neutral $6C-Ag_6$ and $5C-Ag_5$ isomers in water, compared to those in vacuum. Despite some variations in energies and intensities of spectral peaks of different isomers, the overall number of peaks and the spectral profile are quite similar for all isomers in water. This is evidenced by the shape of the spectrum averaged over considered isomers, which coincides well with each individual spectrum of an isomer (dashed magenta lines in Figure 2b,d). As such, the absorption spectra of various DNA—AgNC conformations unlikely result in distinct spectral fingerprints of a specific isomer. On the other hand, presence of different DNA—AgNC isomers in experimental samples is expected to only increase an inhomogeneous broadening of the absorption spectra, while the main absorption features stay nearly the same.

Dependence of Base—Cluster Interactions on the Base Type. Because the Geom-1 and Geom-3 isomers of charged and neutral $6C-Ag_6$ clusters represent two limiting cases for the lowest energy transition being either optically bright or dark, we use these structures as a starting conformation and substitute all six, four, or two cytosines by either guanines (G) or thymines (T) (Table S2 and Figure S3). Figure 3 shows the average binding energy between each base type and Ag_5 or Ag_6 clusters calculated by eq 1 for the most stable isomers of the DNA—AgNCs optimized in water. Both Ag_5 and Ag_6 clusters demonstrate very similar trends in their interactions with nucleobases. For cationic species, the positive charge is distributed over the metal atoms, which increases the interaction between electron-donating Ag and

Figure 2. Absorption spectra of $6C-Ag_6$ isomers: Neutral $6C-Ag_6$ in vacuum (a) and water (b) and charged $6C-Ag_6^+$ in vacuum (c) and water (d). The names of the isomers correspond to those in Table 1. Dashed magenta lines represent the absorption spectra averaged over three isomers. Vertical arrows correspond to the lowest energy optical transition, with the arrow size corresponding to the oscillator strength of the transition.

Ag_5 clusters. The oscillator strength of the lowest energy transition of $6C-Ag_6$ clusters is strongly dependent on the isomer conformation, resulting in a completely optically forbidden (dark) first transition of the Geom-1 isomer and optically allowed (bright) first transition of other neutral isomers both in vacuum and water, Figure 2a,b. Interestingly, Geom-3, the most stable neutral isomer in water, has the bright lowest energy transition, which is expected to provide favorable conditions for high emission of $6C-Ag_6$ clusters in water. In contrast, the Geom-3 isomer of the charged $6C-Ag_6^+$ cluster has the optically dark first transition in water for the most

Figure 3. Binding energy of cytosine, guanine, and thymine to Ag_5 (a) and Ag_6 (b) clusters in water. The most stable isomer of each DNA—AgNC is chosen from the optimized geometry started with either the Geom-3 or Geom-1 structures of neutral and charged $6C-Ag_6$ and $5C-Ag_5$ in water with all or several C substituted by T or G. Neutral cluster are depicted by solid symbols and charged clusters by empty symbols. X-axis indicates the number and types of bases passivating the cluster.

electronegative N and O atoms of the bases.[78,79] As a result, the base−AgNC binding energy is typically stronger in charged clusters, compared to the respective neutral counterparts, Figure 3 and Figure S3. This trend is mostly consistent for cytosines, due to its largest electrostatic dipole moment.[80] Among the considered bases, T−AgNC interaction is the weakest both for neutral and charged clusters, which is rationalized by the smallest dipole moment of T.[80] For the charged clusters, the presence of other base types noticeably reduces the T−AgNC interactions, changing the binding energy from −0.3 eV to −0.05 eV. Such a weak binding energy together with a high flexibility due to a small size of the thymine suggests that thymines are likely weakly contributing to the coordination of AgNC, when strongly interacting cytosines and guanines are present in a DNA strand.

Strongly interacting cytosines also show some decrease in their interactions with the AgNC (changing E_b from −0.6 to −0.5 eV) when other bases passivate the charged cluster, Figure 3. This trend can be rationalized by a reduced number of effective hydrogen bonds formed between bases of different types, which have larger contributions for charged systems compared to neutral clusters in water, Table 2. In contrast, for neutral clusters, the C−AgNC and G−AgNC interactions are enhanced due to other bases. It is known that the dipole moment of a base noticeably changes depending on its location in the DNA sequence or codons[80] and the ionization potential of the nucleotide base pairs.[75] Thus, the dipole moment of G significantly increases when it is paired with C, CC, or CT, compared to GGG; the dipole moment of C also increases when it is paired with T, G, TT, or GG, compared to CCC.[80] By analogy, a presence of other bases at the surface of the AgNC in a close proximity to C or G increases the dipole moment of these bases, resulting in their stronger interactions with the cluster. Overall, the strength of interactions of cytosines and guanines with AgNCs is comparable, with a very slight enhancement for guanines.

It is important to note that for charged clusters $6G−Ag_6^+$ and $4C2G−Ag_6^+$, a strong dipole moment along with a relatively large size of guanines results in a formation of two Ag_3 subclusters that are held together by weak base−base interactions via hydrogen bonds, Figure 1. This result suggests that despite a strong G−AgNC binding energy, the charged clusters coordinated by guanines are less stable compared to those coordinated by cytosines and likely dissociate into several smaller clusters under thermal fluctuations.

Effect of Different Bases on Optical Spectra of Clusters. Absorption spectra of Ag_6 and Ag_6^+ clusters passivated by various bases for the most stable isomers in water are shown in Figure 4. The spectra for all calculated structures are plotted in Figures S4−S6. For all neutral clusters, one can resolve five main absorption bands: (I) a weak peak (or a shoulder) at 2.0−2.9 eV, (II) an intensive peak at ∼3 eV, (III) another intensive peak at ∼3.5 eV, which tends to overlap with the neighboring peak depending on the passivating bases, (IV) a less intensive and broader band at 4.0−4.7 eV, and (V) a highly intensive peak at ∼5.2 eV, Figures 4a,b and S4. While the relative intensity, width, and the energy of the peak maxima are slightly changing depending on the passivating bases and conformations, the overall spectral shape with five well-resolved bands is consistent for all structures. Interestingly, experimental spectra of a bigger Ag_{10}^{6+} cluster formed by repeated CCX sequences where X ≠ C show similar lower energy absorption bands with a weak band at 2.25−2.60 eV
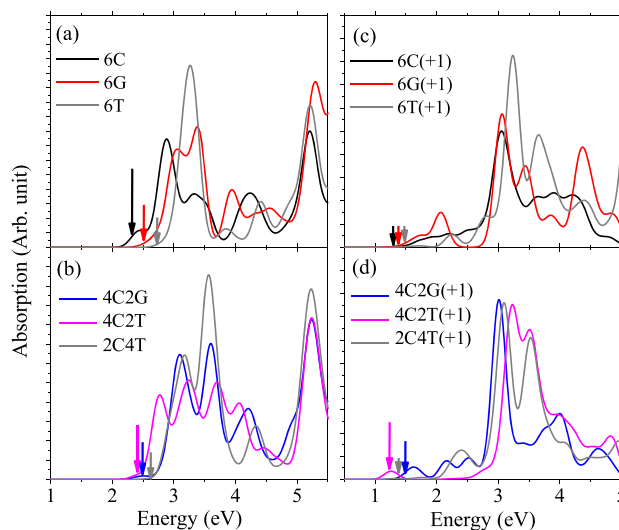
Figure 4. Absorption spectra of Ag_6 and Ag_6^+ clusters passivated by various bases in water. For these spectra, the most stable isomer is chosen from the optimized geometry started with either the Geom-3 or Geom-1 structures of $6C−Ag_6$ (a) and (b) and $6C−Ag_6^+$ (c) and (d) in water with all (a) and (c) or several C (b) and (d) substituted by by T or G. Vertical arrows indicate the lowest energy optical transition. The height of arrows represents the relative intensity of these transitions.

followed by a strong substructured band at 2.75−3.50 eV, with the intensity of the first peak being more sensitive to the sequences and the length of the encapsulated strand.[49]

All these bands are also well pronounced in the calculated spectra of charged Ag_6^+ clusters, being almost independent of the passivated bases and conformations. However, for charged clusters, an additional optically weak band appears at the lower energy range of 1−2 eV, Figures 4c,d and S5. Similar bands nearly at the same energy ranges are observed for spectra of Ag_5 and Ag_5^+ clusters passivated by various bases, but with the opposite trend for neutral and charged clusters: Ag_5 exhibits an additional red-shifted weak peak at 1−2 eV, while the spectra of Ag_5^+ do not have this band, Figure S6. This opposite trend of spectra for charged and neutral Ag_5 and Ag_6 clusters is rationalized by the difference in spin multiplicity of transitions contributing to these optical bands. The absorption spectra of the closed shell Ag_5^+ and Ag_6 systems are governed by singlet transitions, while doublet transitions contribute to spectra of the open shell Ag_5 and Ag_6^+ clusters. Thus, the doublet transitions of clusters with open shell electronic structure results in red-shifted optically weak band at the energy <2.5 eV, almost independent of the cluster size (5 or 6 atoms), its conformation and the passivating bases. However, its intensity and the energy of the peak maximum are sensitive to the base type.

Charge Transfer Character of Optical Transitions of Clusters Passivated by Different Bases. It has been computationally predicted and experimentally detected that the lowest excited states in small emissive AuNCs[81,82] and AgNCs[79,83,84] passivated by various ligands often have the ligand-to-metal charge transfer (LMCT) and metal-to-ligand charge transfer (MLCT) characters. Our calculations demonstrate that the stable isomer of $6C−Ag_6$ has the most intensive first optical transition compared to other stable structures of Ag_6 passivated by different bases, which is expected to lead to

enhanced emission. Such a high intensity is rationalized by the largest MLCT character of this transition, with the hole mainly originating from the metal, while the electron density is locating on both metal atoms and cytosines, as evidenced from NTOs depicted in Table 3 (Ag$_6$ clusters) and Table S3 (Ag$_5$

Table 3. Natural Transition Orbitals Showing the Contributions of the Electron−Hole Pair to the Transitions with the Lowest Energy (S$_1$) and with the Largest Oscillator Strength (Os. Str., italic font) at the Energy Range of 2.5−3.5 eV of the Neutral Ag$_6$ Clusters Passivated by Different Bases in Water with the Most Stable Conformations

State E (eV) Os. Str.	Hole	Electron	State E (eV) f$_{os}$	Hole	Electron
6T			**6C**		
S$_1$ 2.64 eV 0.0014			S$_1$ 2.38 0.0935		
S$_6$ 3.18 eV 0.6339			S$_2$ 2.50 0.0922		
S$_8$ 3.33 eV 1.1471			S$_5$ 2.82 0.4517		
2C4T			**4C2T**		
S$_1$ 2.56 eV 0.0024			S$_1$ 2.41 eV 0.0300		
S$_6$ 3.20 eV 0.7731			S$_8$ 3.30 eV 0.4403		
6G			**4C2G**		
S$_1$ 2.51 eV 0.0171			S$_1$ 2.42 eV 0.0126		
S$_4$ 2.98 eV 0.7135			S$_6$ 3.09 eV 0.7158		

clusters). Changing all or several cytosines to guanines or thymines reduces the ligand contributions to the lowest transition; this in turn decreases the MLCT character, resulting in weaker optical intensities of these transitions. For higher energy optical transitions contributing to the second and third peaks at the energy range of 2.5−3.5 eV, this trend is the same: Optically active transitions with the largest oscillator strengths exhibit stronger MLCT character with a significant portion of the electron density distributed over the base bearing π^* character, Table 3 and Tables S4 and S5.

Figures 5, S7, and S8 quantitatively represent the degree of calculated charge transfer, for each transition obtained for the most stable conformations of the charged and neutral Ag$_6$ clusters passivated by different bases. The degree of charge transfer, $D_m = P_e − P_h$, is identified as a difference between electron and hole orbitals contributing to the excited-state m and integrated over the base or the AgNC fragments, as defined by eqs v−vii in SI. Negative values of D_m indicate the charge transfer from the fragment and positive values of D_m indicate the charge transfer to the fragment. As a result, D_m presented as vertical sticks in Figures 5, S7, and S8 are mirror images of positive and negative values. Very small $|D_m|$ values
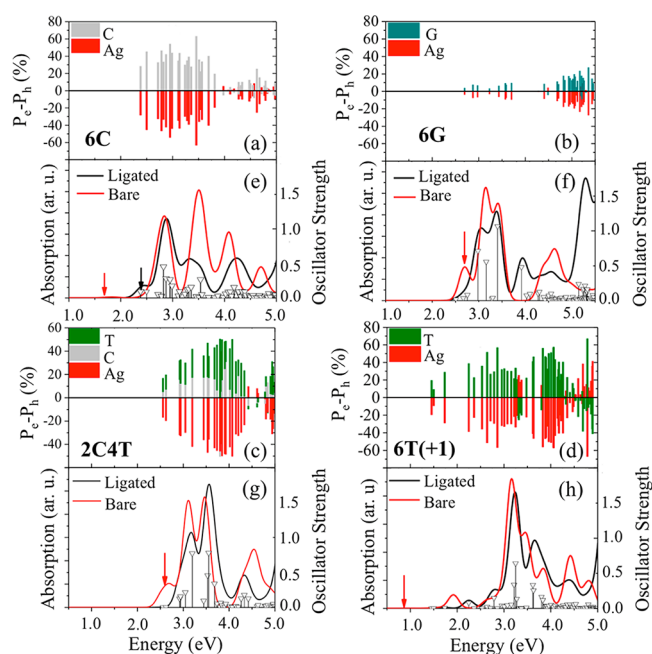
Figure 5. Absorption spectra and percent of charge transfer in each optical transition of the neutral Ag$_6$ and charged Ag$_6^+$ clusters passivated by different bases in water with the most stable conformations. (a−d) The degree of charge transfer, $P_e − P_h$, for each optical transition defined as a difference between projections of unoccupied (electron) and occupied (hole) orbitals projected to the base C (gray), G (teal), or T (green) and the Ag cluster (red). (e−h) Absorption spectra of the optimized clusters passivated by bases (black lines) and the bare cluster with eliminated bases but preserving the same geometry as it has in the passivated structures (red line). Vertical black lines with triangle heads identify the oscillator strength of each optical transition contributing to the absorption spectra of the passivated clusters. The values of the oscillator strength are represented at the right Y-axis. Red arrows indicate the lowest energy transition of the cluster with removed bases.

indicate that transitions have negligible CT character and are mainly metal-to-metal or base-to-base ($\pi−\pi^*$) transitions.

For all structures, according to this analysis, optical transitions with energies <4 eV exhibit a noticeable degree of MLCT character ranging from 20% to 60%. The lowest energy transitions have the largest degree of MLCT (up to 40%) for **6C**-Ag$_6$ and the smallest for **6G**-Ag$_6$ (∼10%), Figure 5a−d. The absorption bands at ∼3.5 eV have the largest MLCT character up to 55% for all structures, except **6G**-Ag$_6$ that has the MLCT degree <20% for all transitions at this energy range, Figure S7. In contrast to all other neutral clusters, the optical bands at 2.5−3.5 eV of **6G**-Ag$_6$ are predominantly metal-to-metal transitions, which is also confirmed by NTOs depicted in Table 3. We associate such a low degree of MLCT with the bulkiness of guanines, having size that is larger than the cluster size, hindering the hybridization of orbitals between guanines and the cluster. It is important to note that the MLCT character of the lowest transitions increases when guanines or thymines are accompanied by cytosines (**4C2G**- and **4C2T**−Ag$_6$), Figure S7. This increase in MLCT character is reflected by higher intensities of these transitions compared to those of **6G**-, **6T**-, and **2C4T**−Ag$_6$, Figure 4a,b. Nonetheless, the MLCT character mainly originates from cytosines (∼30%), with less than 10% contributions from the other bases. Thus,

Table 4. Decomposition of the NTO Electron−Hole Pair over the Ag-Associated s, p, and d Angular Momentum Contributions to the Excited State of the Most Stable Ag$_6$ Clusters Ligated by Different Bases and Their Bare Ag$_6$ Counterparts[a]

cluster	h/e pairs at 2.0−3.0 eV			h/e pairs at 3.0−3.5 eV			h/e pairs at 3.5−4.5 eV		
	s	p	d	s	p	d	s	p	d
6C	**50/25**	20/30	15/5	**60/15**	10/25	10/5	**55/35**	20/55	10/0
bare	**80/60**	10/30	10/10	**80/15**	10/80	10/5	**80/25**	10/80	10/0
6T	**65/35**	15/35	5/5	**70/20**	15/35	5/5	**70/40**	15/50	5/0
bare	**85/70**	10/20	5/5	**85/40**	10/55	5/5	**80/30**	10/70	5/0
6G	**60/20**	15/50	10/5	**60/25**	15/45	10/5	**60/15**	15/75	10/0
bare	**85/70**	10/30	5/5	**85/40**	10/70	5/5	**85/20**	10/80	5/0
4C2G	**55/25**	20/30	5/5	**60/15**	15/30	10/5	**60/35**	20/60	10/0
bare	**80/70**	10/20	10/5	**80/45**	15/50	5/5	**80/20**	10/80	10/0
4C2T	**65/15**	20/30	5/5	**60/15**	15/30	10/5	**60/30**	20/55	10/0
bare	**80/70**	10/25	10/5	**80/45**	10/50	5/5	**80/25**	10/75	10/0
2C4T	**65/25**	15/35	10/5	**60/20**	15/30	10/5	**65/15**	15/55	10/0
bare	**80/70**	10/25	5/5	**80/30**	10/65	5/5	**80/15**	10/85	5/0

[a]The percents of s, p, and d in hole (h) and electron (e) states are integrated over the energy range corresponding to the main optical bands in Figure 4. The bold font highlights the dominant percent of the orbital type in the hole/electron pair.

cytosines maintain the MLCT character of the lowest energy transitions to a higher degree compared to the other bases.

We also compare the absorption spectra of the passivated Ag$_6$ clusters and the bare clusters in which the passivated bases are deleted, while the cluster is preserving the same geometry as it has in the passivated arrangement, Figures 5e−h and S7. Interestingly, the lowest energy transitions of the neutral bare clusters are optically active, in contrast to those of the passivated clusters, except **6C**−Ag$_6$. For the latter, the passivated cluster has an optically active first transition, while it is optically inactive for the bare cluster. These opposite trends point to a change in the optical selection rules of the lowest transitions of AgNCs due to delocalization of the excited state both over the cluster and the bases underpinning the MLCT character. In contrast, highly intensive absorption peaks at 3.0−3.5 eV almost coincide between the bare and the passivated clusters especially in **6G**-, **6T**-, and **2C4T**−Ag$_6$, despite the admixture of MLCT character of transitions contributing to these peaks, Figures 5a−d and S7. As such, transitions at this energy range exhibit similar optical selection rules for both pure metal-to-metal and mixed MLCT states.

The consistency in the behavior of transitions at 3.0−3.5 eV between the bare and ligated clusters can be rationalized by similarities in contributions of s, p, and d orbitals of Ag atoms to the optical transitions for both ligated and bare clusters, Table 4 and Figure S9. At this energy range, both the bare and ligated clusters demonstrate the predominant s character (60−85%) of holes and mainly p character of electrons, with variations of 55−80% for the bare Ag$_6$ and 25−45% for the ligated clusters. A small admixture of d orbitals (5−10%) is also observed for both electron and hole states contributing to the optical bands at 3.0−3.5 eV. Note that the values corresponding to electrons are significantly smaller for the ligated clusters, compared to their bare counterparts, due to the redistribution of some portion of the orbital to the bases. Relatively delocalized character of p orbitals distributed over more Ag atoms facilitates the delocalization of electrons to the passivating bases, while more localized nature of s orbitals locates the hole at the metal center, thus facilitating strong MLCT character of this spectral band.

Similar to transitions at 3.0−3.5 eV, the lowest energy transitions contributing to the 2.5−3.0 eV band of the ligated

clusters also exhibit the s character of holes (50−70%) and p character of electrons (30−50%), but with a more pronounced admixture of s orbitals in the electron states, Table 4. In contrast, the lowest transitions in the bare clusters show smaller contributions of p orbitals to electrons resulting in a predominant s character of both electrons (60−70%) and holes (80−85%), Table 4 and Figure S9. These results agree with literature reports showing that the lower energy transitions in bare silver clusters with less than eight atoms in size mainly involve s orbitals, where the hole has predominantly s orbital contribution and the electron has a more hybridized s + p character.[85,86] However, a significantly stronger degree of s + p character of electrons in the ligated clusters, compared to their bare counterparts, is responsible for differences in their optical selection rules defining the lowest transition intensities for the 2.0−3.0 eV band.

The absorption band at 4.0−4.5 eV has the smallest MLCT contribution (<20%) for all ligated structures, Figures 5a−c and S7. The relevant NTOs demonstrate either π−π* transitions originated from bases or metal originated transitions with predominant s character of holes and p character with a very small admixture of s orbitals of electrons, similar to the bare clusters, Table 4. Notably, there are no d orbital contributions to the electron states for both ligated and bare clusters, Table 4 and Figure S9. A lack of d character also reflects on the reduced MLCT character of these transitions in the ligated systems. Due to the reduced hybridization of the electron−hole pairs, the intensity of these transitions is noticeably smaller compared to those in the 3.0−3.5 eV range. Comparing the bare and ligated structures, there is a significant splitting between optical peaks at ∼4.0 eV in the bare clusters, which is not present in the ligated clusters. This is a result of minimizing the energy splitting between the bonding and antibonding Ag-associated p orbitals due to the perturbation by nucleobases' electrostatic dipoles,[86] despite a minimal direct contribution of base orbitals to these states. This explains significant deviations between this band in the bare and passivated clusters, Figures 5e−h and S7.

For the band at the energy >4.5 eV, the CT degree increases to 20−40% for most structures but exhibiting mainly LMCT rather than MLCT character. For these transitions, the d orbital contribution to holes becomes significant (40−80%),

Table 4 and Figure S9. These results agree well with previously reported calculations of DNA−Ag$_4$ clusters, showing that the absorption peaks from red to blue wavelengths are predominantly of MLCT character, while absorption in the blue-violet range are mostly represented by transitions with a mixed character of LMCT or d-d* nature.[68] The similar trends in CT contributions to all absorption bands are observed for charged passivated and bare Ag$_6^+$ clusters, with the difference that the lowest energy optically inactive transition (at ∼1.5 eV) has a small contribution of MLCT with a dominant metal-to-metal character associated with s orbitals of both electrons and holes, Figures S8 and S10.

CONCLUSIONS

We have performed a computational study aiming to clarify how the differences in conformations, charges, solvent polarity, and passivating bases impact optical spectra of DNA−AgNCs systems containing five and six Ag atoms. Our calculations demonstrate that a polar solvent such as water is an important factor that transforms the geometries of clusters passivated by cytosines from planar 2-D to nonplanar 3-D structures, while the planar conformations are most stable for the nonpassivated Ag$_5$ and Ag$_6$ clusters.[56] In addition to the cluster−base interactions, the hydrogen bond network between passivating bases significantly impacts the cluster geometry and its stability. Therefore, the most stable isomer is characterized by the largest number of hydrogen bonds and the strongest base−cluster interactions. It is likely that several isomers of base-passivated clusters coexist in polar solvents due to the relatively small ground-state energy differences between their conformations (<0.2 eV). Comparing the cluster−base binding energies, cytosines and guanines interact much stronger than thymines even in mixed passivations, due to their larger electrostatic dipole moments. These interactions are increasing in cationic clusters. Almost twice weaker binding energy of T, compared to C and G, suggests that thymines likely contribute a little to the coordination of AgNCs, when cytosines and guanines are present in a DNA strand.

Despite some variations in energies and intensities of spectral peaks of clusters with different conformations, passivation bases, and charges, the spectral absorption profile with five well-resolved main peaks at the range of 2.5−5.5 eV is common for all studied structures. As such, the optical spectrum of various DNA−AgNC species will unlikely result in distinct spectral fingerprints defined by a specific conformation or a base-type passivation. The exception is observed for clusters with the open shell electronic structure. Our calculations reveal that the doublet transitions in base-passivated clusters with the open shell electronic structure (Ag$_5$ and Ag$_6^+$) result in an additional red-shifted (<2.5 eV) and optically weak band. Transitions contributing to this band show a small MLCT character with a dominant metal-to-metal nature associated with s orbitals for both electrons and holes. However, the passivated clusters with the closed shell electronic structure (Ag$_5^+$ and Ag$_6$) exhibit higher optical intensity of their lowest transitions with a high MLCT contribution, thus having superior potential for emission, than their open shell counterparts.

For all considered structures, optical transitions at 2.5−3.5 eV exhibit a strong MLCT character with the main contribution stemming from the Ag-core to the bases. Cytosines facilitate the MLCT character to a larger degree compared to guanines and thymines, including the mixed

nucleobase passivation. The MLCT character of these transitions is rationalized by the s+p+d hybridized nature of the excited electron, which is distributed over multiple Ag atoms, facilitating the delocalization of the electron density to the passivating bases; in contrast, the more localized nature of s orbitals, mainly contributing to the hole state, locates the hole density at the metal center. The most optically active transitions expose the largest degree of MLCT with a significant portion of the electron density distributed over the base bearing π* character. In contrast, the higher energy absorption band at 4.0−4.5 eV has a weak optical intensity, which we attribute to a lower degree of MLCT character to these transitions. This is also rationalized by a reduced hybridization of electron states lacking d orbital contributions, while dominated by p orbitals. For the optically intensive band at the energy >5.0 eV, the charge transfer character increases, while retaining mainly LMCT rather than MLCT features. This change is dictated by significantly increased contributions of d orbitals to hole states, leading to delocalization of the hole between metal center and bases. Overall, our results facilitate better understanding of the intrinsic properties of DNA−AgNCs chromophores and provide guidelines to new experimental studies targeting specific optical functions of silver-based biologically compatible nanosystems.

ASSOCIATED CONTENT

Supporting Information

The Supporting Information is available free of charge at https://pubs.acs.org/doi/10.1021/acs.jpca.0c06974.

Structural parameters, binding energy and its discussion, absorption spectra of 5C−Ag$_5$ isomers, binding energies of Ag$_5$ and Ag$_6$ clusters in water, absorption spectra of the conformations of mixed nucleobase, NTOs, degree of charge transfer, and angular momentum contributions (PDF)

AUTHOR INFORMATION

Corresponding Author

Svetlana Kilina − *Department of Chemistry and Biochemistry, North Dakota State University, Fargo, North Dakota 58108, United States;* ⓞ orcid.org/0000-0003-1350-2790; Email: Svetlana.Kilina@ndsu.edu

Authors

Mohammed A. Jabed − *Department of Chemistry and Biochemistry, North Dakota State University, Fargo, North Dakota 58108, United States;* ⓞ orcid.org/0000-0001-8552-0301

Naveen Dandu − *Argonne National Laboratory, Lemont, Illinois 60439, United States;* ⓞ orcid.org/0000-0001-7122-8537

Sergei Tretiak − *Center for Nonlinear Studies, Center for Integrated Nanotechnologies, and Theoretical Division, Los Alamos National Laboratory, Los Alamos, New Mexico 87545, United States;* ⓞ orcid.org/0000-0001-5547-3647

Complete contact information is available at:
https://pubs.acs.org/10.1021/acs.jpca.0c06974

Notes

The authors declare no competing financial interest.

REFERENCES

(1) Petty, J. T.; Zheng, J.; Hud, N. V.; Dickson, R. M. DNA-Templated Ag Nanocluster Formation. *J. Am. Chem. Soc.* **2004**, *126*, 5207−5212.

(2) Schultz, D.; Gardner, K.; Oemrawsingh, S. S.; Markesevic, N.; Olsson, K.; Debord, M.; Bouwmeester, D.; Gwinn, E. Evidence for Rod-shaped DNA-stabilized Silver Nanocluster Emitters. *Adv. Mater.* **2013**, *25*, 2797−803.

(3) Liu, J. DNA-stabilized, Fluorescent, Metal Nanoclusters for Biosensor Development. *TrAC, Trends Anal. Chem.* **2014**, *58*, 99−111.

(4) Gwinn, E.; Schultz, D.; Copp, S. M.; Swasey, S. DNA-Protected Silver Clusters for Nanophotonics. *Nanomaterials* **2015**, *5*, 180−207.

(5) Han, B.; Wang, E. DNA-templated Fluorescent Silver Nanoclusters. *Anal. Bioanal. Chem.* **2012**, *402*, 129−138.

(6) Latorre, A.; Somoza, A. DNA-mediated Silver Nanoclusters: Synthesis, Properties and Applications. *ChemBioChem* **2012**, *13*, 951−958.

(7) Obliosca, M. J.; Liu, C.; Batson, A. R.; Babin, C. M.; Werner, H. J.; Yeh, H.-C. DNA/RNA Detection Using DNA-Templated Few-Atom Silver Nanoclusters. *Biosensors* **2013**, *3*, 185−200.

(8) Petty, J. T.; Story, S. P.; Hsiang, J.-C.; Dickson, R. M. DNA-Templated Molecular Silver Fluorophores. *J. Phys. Chem. Lett.* **2013**, *4*, 1148−1155.

(9) Goswami, N.; Zheng, K.; Xie, J. Bio-NCs − the Marriage of Ultrasmall Metal Nanoclusters with BioMolecules. *Nanoscale* **2014**, *6*, 13328−13347.

(10) Richards, C. I.; Choi, S.; Hsiang, J.-C.; Antoku, Y.; Vosch, T.; Bongiorno, A.; Tzeng, Y.-L.; Dickson, R. M. Oligonucleotide-Stabilized Ag Nanocluster Fluorophores. *J. Am. Chem. Soc.* **2008**, *130*, 5038−5039.

(11) Berti, L.; Burley, G. A. Nucleic Acid and Nucleotide-mediated Synthesis of Inorganic Nanoparticles. *Nat. Nanotechnol.* **2008**, *3*, 81.

(12) Díez, I.; Ras, R. H. A.; Kanyuk, M. I.; Demchenko, A. P. On Heterogeneity in Fluorescent Few-Atom Silver Nanoclusters. *Phys. Chem. Chem. Phys.* **2013**, *15*, 979−985.

(13) Ritchie, C. M.; Johnsen, K. R.; Kiser, J. R.; Antoku, Y.; Dickson, R. M.; Petty, J. T. Ag Nanocluster Formation Using a Cytosine Oligonucleotide Template. *J. Phys. Chem. C* **2007**, *111*, 175−181.

(14) Shang, L.; Dong, S. Facile Preparation of Water-soluble Fluorescent Silver Nanoclusters using a Polyelectrolyte Template. *Chem. Commun.* **2008**, No. 9, 1088−1090.

(15) Yang, C.; Shi, K.; Dou, B.; Xiang, Y.; Chai, Y.; Yuan, R. In Situ DNA-Templated Synthesis of Silver Nanoclusters for Ultrasensitive and Label-Free Electrochemical Detection of MicroRNA. *ACS Appl. Mater. Interfaces* **2015**, *7*, 1188−1193.

(16) Shen, C.; Xia, X.; Hu, S.; Yang, M.; Wang, J. Silver Nanoclusters-Based Fluorescence Assay of Protein Kinase Activity and Inhibition. *Anal. Chem.* **2015**, *87*, 693−698.

(17) Wang, Y.; Dai, C.; Yan, X.-P. Fabrication of Folate Bioconjugated Near-infrared Fluorescent Silver Nanoclusters for Targeted in Vitro and in Vivo Bioimaging. *Chem. Commun.* **2014**, *50*, 14341−14344.

(18) Li, J.; You, J.; Dai, Y.; Shi, M.; Han, C.; Xu, K. Gadolinium Oxide Nanoparticles and Aptamer-Functionalized Silver Nanoclusters-Based Multimodal Molecular Imaging Nanoprobe for Optical/Magnetic Resonance Cancer Cell Imaging. *Anal. Chem.* **2014**, *86*, 11306−11311.

(19) Supran, G. J.; Song, K. W.; Hwang, G. W.; Correa, R. E.; Scherer, J.; Dauler, E. A.; Shirasaki, Y.; Bawendi, M. G.; Bulović, V. High-Performance Shortwave-Infrared Light-Emitting Devices Using Core-Shell (PbS-CdS) Colloidal Quantum Dots. *Adv. Mater.* **2015**, *27*, 1437−1442.

(20) Su, Y.-T.; Lan, G.-Y.; Chen, W.-Y.; Chang, H.-T. Detection of Copper Ions Through Recovery of the Fluorescence of DNA-Templated Copper/Silver Nanoclusters in the Presence of Mercaptopropionic Acid. *Anal. Chem.* **2010**, *82*, 8566−8572.

(21) Chen, W.-Y.; Lan, G.-Y.; Chang, H.-T. Use of Fluorescent DNA-Templated Gold/Silver Nanoclusters for the Detection of Sulfide Ions. *Anal. Chem.* **2011**, *83*, 9450−9455.

(22) Chen, Y.-A.; Obliosca, J. M.; Liu, Y.-L.; Liu, C.; Gwozdz, M. L.; Yeh, T. Nanocluster Beacons for Detection of a Single N6-Methyladenine Epigenetic Modification. *Biophys. J.* **2016**, *110*, 519a.

(23) Jain, P. K.; Huang, X.; El-Sayed, I. H.; El-Sayed, M. A. Noble Metals on the Nanoscale: Optical and Photothermal Properties and Some Applications in Imaging, Sensing, Biology, and Medicine. *Acc. Chem. Res.* **2008**, *41*, 1578−1586.

(24) Lohse, S. E.; Murphy, C. J. Applications of Colloidal Inorganic Nanoparticles: From Medicine to Energy. *J. Am. Chem. Soc.* **2012**, *134*, 15607−15620.

(25) Richards, C. I.; Hsiang, J.-C.; Senapati, D.; Patel, S.; Yu, J.; Vosch, T.; Dickson, R. M. Optically Modulated Fluorophores for Selective Fluorescence Signal Recovery. *J. Am. Chem. Soc.* **2009**, *131*, 4619−4621.

(26) Cerretani, C.; Carro-Temboury, M. R.; Krause, S.; Bogh, S. A.; Vosch, T. Temperature dependent excited state relaxation of a red emitting DNA-templated Silver Nanocluster. *Chem. Commun.* **2017**, *53*, 12556−12559.

(27) Gwinn, E. G.; O'Neill, P.; Guerrero, A. J.; Bouwmeester, D.; Fygenson, D. K. Sequence-Dependent Fluorescence of DNA-Hosted Silver Nanoclusters. *Adv. Mater.* **2008**, *20*, 279−283.

(28) Li, Y.; Wang, X.; Xu, S.; Xu, W. The Solvent Effect on the Luminescence of Silver Nanoclusters. *Phys. Chem. Chem. Phys.* **2013**, *15*, 2665−2668.

(29) Copp, S. M.; Schultz, D.; Swasey, S. M.; Faris, A.; Gwinn, E. G. Cluster Plasmonics: Dielectric and Shape Effects on DNA-Stabilized Silver Clusters. *Nano Lett.* **2016**, *16*, 3594−3599.

(30) Schultz, D.; Gwinn, E. G. Silver Atom and Strand Numbers in Fluorescent and Dark Ag:DNAs. *Chem. Commun.* **2012**, *48*, 5748−5750.

(31) Copp, S. M.; Schultz, D.; Swasey, S.; Pavlovich, J.; Debord, M.; Chiu, A.; Olsson, K.; Gwinn, E. Magic Numbers in DNA-Stabilized Fluorescent Silver Clusters Lead to Magic Colors. *J. Phys. Chem. Lett.* **2014**, *5*, 959−963.

(32) Zheng, J.; Nicovich, P. R.; Dickson, R. M. Highly Fluorescent Noble-metal Quantum Dots. *Annu. Rev. Phys. Chem.* **2007**, *58*, 409−431.

(33) Schmid, G. Large clusters and colloids. Metals in the Embryonic State. *Chem. Rev.* **1992**, *92*, 1709−1727.

(34) Aikens, C. M. Electronic Structure of Ligand-Passivated Gold and Silver Nanoclusters. *J. Phys. Chem. Lett.* **2011**, *2*, 99−104.

(35) Bogh, S. A.; Cerretani, C.; Kacenauskaite, L.; Carro-Temboury, M. R.; Vosch, T. Excited-State Relaxation and Förster Resonance Energy Transfer in an Organic Fluorophore/Silver Nanocluster Dyad. *ACS Omega* **2017**, *2*, 4657−4664.

(36) Wang, K.-H.; Chang, C.-W. The Spectral Relaxation Dynamics and the Molecular Crowding Effect of Silver Nanoclusters

Synthesized in the Polymer Scaffold. *Phys. Chem. Chem. Phys.* **2015**, *17*, 23140−23146.

(37) Hooley, E. N.; Carro-Temboury, M. R.; Vosch, T. Probing the Absorption and Emission Transition Dipole Moment of DNA Stabilized Silver Nanoclusters. *J. Phys. Chem. A* **2017**, *121*, 963−968.

(38) Ganguly, M.; Bradsher, C.; Goodwin, P.; Petty, J. T. DNA-Directed Fluorescence Switching of Silver Clusters. *J. Phys. Chem. C* **2015**, *119*, 27829−27837.

(39) Yeh, H.-C.; Sharma, J.; Han, J. J.; Martinez, J. S.; Werner, J. H. A DNA−Silver Nanocluster Probe That Fluoresces upon Hybridization. *Nano Lett.* **2010**, *10*, 3106−3110.

(40) Driehorst, T.; O'Neill, P.; Goodwin, P. M.; Pennathur, S.; Fygenson, D. K. Distinct Conformations of DNA-Stabilized Fluorescent Silver Nanoclusters Revealed by Electrophoretic Mobility and Diffusivity Measurements. *Langmuir* **2011**, *27*, 8923−8933.

(41) Link, S.; Wang, Z. L.; El-Sayed, M. A. Alloy Formation of Gold−Silver Nanoparticles and the Dependence of the Plasmon Absorption on Their Composition. *J. Phys. Chem. B* **1999**, *103*, 3529−3533.

(42) Petty, J. T.; Nicholson, D. A.; Sergev, O. O.; Graham, S. K. Near-Infrared Silver Cluster Optically Signaling Oligonucleotide Hybridization and Assembling Two DNA Hosts. *Anal. Chem.* **2014**, *86*, 9220−9228.

(43) Choi, S.; Yu, J.; Patel, S. A.; Tzeng, Y.-L.; Dickson, R. M. Tailoring Silver Nanodots for Intracellular Staining. *Photochem. Photobiol. Sci.* **2011**, *10*, 109−115.

(44) Morishita, K.; MacLean, J. L.; Liu, B.; Jiang, H.; Liu, J. Correlation of Photobleaching, Oxidation and Metal Induced Fluorescence Quenching of DNA-templated Silver Nanoclusters. *Nanoscale* **2013**, *5*, 2840−2849.

(45) Sengupta, B.; Springer, K.; Buckman, J. G.; Story, S. P.; Abe, O. H.; Hasan, Z. W.; Prudowsky, Z. D.; Rudisill, S. E.; Degtyareva, N. N.; Petty, J. T. DNA Templates for Fluorescent Silver Clusters and i-motif Folding. *J. Phys. Chem. C* **2009**, *113*, 19518−19524.

(46) Ma, K.; Shao, Y.; Cui, Q.; Wu, F.; Xu, S.; Liu, G. Base-Stacking-Determined Fluorescence Emission of DNA Abasic Site-Templated Silver Nanoclusters. *Langmuir* **2012**, *28*, 15313−15322.

(47) Ramazanov, R. R.; Sych, T. S.; Reveguk, Z. V.; Maksimov, D. A.; Vdovichev, A. A.; Kononov, A. I. Ag−DNA Emitter: Metal Nanorod or SupraMolecular Complex? *J. Phys. Chem. Lett.* **2016**, *7*, 3560−3566.

(48) Petty, J. T.; Sergev, O. O.; Ganguly, M.; Rankine, I. J.; Chevrier, D. M.; Zhang, P. A Segregated, Partially Oxidized, and Compact Ag10 Cluster within an Encapsulating DNA Host. *J. Am. Chem. Soc.* **2016**, *138*, 3469−3477.

(49) Petty, J. T.; Ganguly, M.; Rankine, I. J.; Baucum, E. J.; Gillan, M. J.; Eddy, L. E.; Léon, J. C.; Müller, J. Repeated and Folded DNA Sequences and Their Modular Ag106+ Cluster. *J. Phys. Chem. C* **2018**, *122*, 4670−4680.

(50) Schultz, D.; Gwinn, E. Stabilization of Fluorescent Silver Clusters by RNA Homopolymers and their DNA Analogs: C, G versus A, T (U) Dichotomy. *Chem. Commun.* **2011**, *47*, 4715−4717.

(51) Soto-Verdugo, V.; Metiu, H.; Gwinn, E. The Properties of Small Ag Clusters Bound to DNA Bases. *J. Chem. Phys.* **2010**, *132*, 195102.

(52) Swasey, S. M.; Leal, L. E.; Lopez-Acevedo, O.; Pavlovich, J.; Gwinn, E. G. Silver (I) as DNA Glue: Ag+ Mediated Guanine Pairing Revealed by Removing Watson-Crick Constraints. *Sci. Rep.* **2015**, *5*, 10163.

(53) Dale, B. B.; Senanayake, R. D.; Aikens, C. M. Research Update: Density Functional Theory Investigation of the Interactions of Silver Nanoclusters with Guanine. *APL Mater.* **2017**, *5*, 053102.

(54) Chen, T.-T.; Chen, Q.-Y.; Liu, M.-Y. GAG-containing Nucleotides as Mediators of DNA-Silver Clusters and Iron-DNA Interplay. *Chin. Chem. Lett.* **2016**, *27*, 395−398.

(55) Brown, S. L.; Hobbie, E. K.; Tretiak, S.; Kilin, D. S. First-Principles Study of Fluorescence in Silver Nanoclusters. *J. Phys. Chem. C* **2017**, *121*, 23875−23885.

(56) Fernández, E. M.; Soler, J. M.; Garzón, I. L.; Balbás, L. C. Trends in the Structure and Bonding of Noble Metal Clusters. *Phys. Rev. B: Condens. Matter Mater. Phys.* **2004**, *70*, 165403.

(57) Samanta, P. K.; Periyasamy, G.; Manna, A. K.; Pati, S. K. Computational Studies on Structural and Optical Properties of Single-stranded DNA Encapsulated Silver/gold Clusters. *J. Mater. Chem.* **2012**, *22*, 6774−6781.

(58) Tsuneda, T. Theoretical Investigations on Geometrical and Electronic Structures of Silver Clusters. *J. Comput. Chem.* **2019**, *40*, 206−211.

(59) Bonačić-Koutecky, V.; Veyret, V.; Mitrić, R. Ab initio Study of the Absorption Spectra of Ag$_n$ (n = 5−8) Clusters. *J. Chem. Phys.* **2001**, *115*, 10450−10460.

(60) Chen, M.; Dyer, J. E.; Li, K.; Dixon, D. A. Prediction of Structures and Atomization Energies of Small Silver Clusters, (Ag)n, *n* < 100. *J. Phys. Chem. A* **2013**, *117*, 8298−8313.

(61) Furche, F.; Ahlrichs, R. Adiabatic Time-dependent Density Functional Methods for Excited State Properties. *J. Chem. Phys.* **2002**, *117*, 7433−7447.

(62) Casida, M. E.; Jamorski, C.; Casida, K. C.; Salahub, D. R. Molecular Excitation Energies to High-lying Bound States from Time-dependent Density-Functional Response Theory: Characterization and Correction of the Time-dependent Local Density Approximation Ionization Threshold. *J. Chem. Phys.* **1998**, *108*, 4439−4449.

(63) Frisch, M. J.; Trucks, G. W.; Schlegel, H. B.; Scuseria, G. E.; Robb, M. A.; Cheeseman, J. R.; Scalmani, G.; Barone, V.; Mennucci, B.; Petersson, G. A.et al. *Gaussian 09*; Gaussian, Inc.: Wallingford, CT, 2009.

(64) Yanai, T.; Tew, D. P.; Handy, N. C. A New Hybrid Exchange−correlation Functional Using the Coulomb-attenuating Method (CAM-B3LYP). *Chem. Phys. Lett.* **2004**, *393*, 51−57.

(65) Hay, P. J.; Wadt, W. R. Ab initio Effective Core Potentials for Molecular Calculations. Potentials for the Transition Metal Atoms Sc to Hg. *J. Chem. Phys.* **1985**, *82*, 270−283.

(66) Ditchfield, R.; Hehre, W. J.; Pople, J. A. Self-Consistent Molecular-Orbital Methods. IX. An Extended Gaussian-Type Basis for Molecular-Orbital Studies of Organic Molecules. *J. Chem. Phys.* **1971**, *54*, 724−728.

(67) Pakiari, A. H.; Jamshidi, Z. Nature and Strength of M−S Bonds (M = Au, Ag, and Cu) in Binary Alloy Gold Clusters. *J. Phys. Chem. A* **2010**, *114*, 9212−9221.

(68) Longuinhos, R.; Lúcio, A. D.; Chacham, H.; Alexandre, S. S. Charge-transfer Optical Absorption Mechanism of DNA:Ag-Nanocluster Complexes. *Phys. Rev. E: Stat. Phys., Plasmas, Fluids, Relat. Interdisc. Top.* **2016**, *93*, 052413.

(69) Ramazanov, R. R.; Kononov, A. I. Excitation Spectra Argue for Threadlike Shape of DNA-Stabilized Silver Fluorescent Clusters. *J. Phys. Chem. C* **2013**, *117*, 18681−18687.

(70) Cossi, M.; Rega, N.; Scalmani, G.; Barone, V. Energies, Structures, and Electronic Properties of Molecules in Solution with the C-PCM Solvation Model. *J. Comput. Chem.* **2003**, *24*, 669−681.

(71) Martin, R. L. Natural Transition Orbitals. *J. Chem. Phys.* **2003**, *118*, 4775.

(72) Humphrey, W.; Dalke, A.; Schulten, K. VMD: Visual Molecular Dynamics. *J. Mol. Graphics* **1996**, *14*, 33−38.

(73) Xiong, R.; Die, D.; Xiao, L.; Xu, Y.-G.; Shen, X.-Y. Probing the Structural, Electronic, and Magnetic Properties of Agn (n = 1−12) Clusters. *Nanoscale Res. Lett.* **2017**, *12*, 625.

(74) Wang, J.; Wang, G.; Zhao, J. Structures and Electronic Properties of Cu20, Ag20, and Au20 Clusters with Density Functional Method. *Chem. Phys. Lett.* **2003**, *380*, 716−720.

(75) Colson, A. O.; Besler, B.; Sevilla, M. D. Ab initio Molecular Orbital Calculations on DNA Base Pair Radical Ions: Effect of Base Pairing on Proton-transfer Energies, Electron Affinities, and Ionization Potentials. *J. Phys. Chem.* **1992**, *96*, 9787−9794.

(76) Itoh, M.; Kumar, V.; Adschiri, T.; Kawazoe, Y. Comprehensive Study of Sodium, Copper, and Silver Clusters Over a Wide Range of Sizes 2 ≤ N ≤ 75. *J. Chem. Phys.* **2009**, *131*, 174510.

(77) Weis, P.; Bierweiler, T.; Gilb, S.; Kappes, M. M. Structures of Small Silver Cluster Cations (Agn+, *n* < 12): Ion Mobility Measurements Versus Density Functional and MP2 Calculations. *Chem. Phys. Lett.* **2002**, *355*, 355−364.

(78) Negishi, Y.; Nobusada, K.; Tsukuda, T. Glutathione-Protected Gold Clusters Revisited: Bridging the Gap between Gold(I)−Thiolate Complexes and Thiolate-Protected Gold Nanocrystals. *J. Am. Chem. Soc.* **2005**, *127*, 5261−5270.

(79) Samanta, P. K.; Manna, A. K.; Pati, S. K. Structural, Electronic, and Optical Properties of Metallo Base Pairs in Duplex DNA: A Theoretical Insight. *Chem. - Asian J.* **2012**, *7*, 2718−2728.

(80) Berezhnoy, A. Y.; Duplij, S. A. Dependence of Nucleotide Physical Properties on their Placement in Codons and Determinative Degree. *J. Zhejiang Univ., Sci.* **2005**, *6*, 948.

(81) Wu, Z.; Jin, R. On the Ligand's Role in the Fluorescence of Gold Nanoclusters. *Nano Lett.* **2010**, *10*, 2568−2573.

(82) Stamplecoskie, K. G.; Kamat, P. V. Size-Dependent Excited State Behavior of Glutathione-Capped Gold Clusters and Their Light-Harvesting Capacity. *J. Am. Chem. Soc.* **2014**, *136*, 11093−11099.

(83) Chen, Y.; Yang, T.; Pan, H.; Yuan, Y.; Chen, L.; Liu, M.; Zhang, K.; Zhang, S.; Wu, P.; Xu, J. Photoemission Mechanism of Water-Soluble Silver Nanoclusters: Ligand-to-Metal−Metal Charge Transfer vs Strong Coupling between Surface Plasmon and Emitters. *J. Am. Chem. Soc.* **2014**, *136*, 1686−1689.

(84) Rodolphe, A.; Thibault, T.; Michel, B.; Philippe, D.; Roland, M.; Vlasta, B.-K. Optical Properties of Gas-Phase Tryptophan−Silver Cations: Charge Transfer from the Indole Ring to the Silver Atom. *ChemPhysChem* **2006**, *7*, 524−528.

(85) Harb, M.; Rabilloud, F.; Simon, D.; Rydlo, A.; Lecoultre, S.; Conus, F.; Rodrigues, V.; Félix, C. Optical Absorption of Small Silver Clusters: Agn, (n = 4−22). *J. Chem. Phys.* **2008**, *129*, 194108.

(86) Grandjean, D.; Coutiño-Gonzalez, E.; Cuong, N. T.; Fron, E.; Baekelant, W.; Aghakhani, S.; Schlexer, P.; D'Acapito, F.; Banerjee, D.; Roeffaers, M. B. J.; Nguyen, M. T.; Hofkens, J.; Lievens, P. Origin of the Bright Photoluminescence of Few-atom Silver Clusters Confined in LTA Zeolites. *Science* **2018**, *361*, 686−690.